Accepted Manuscript

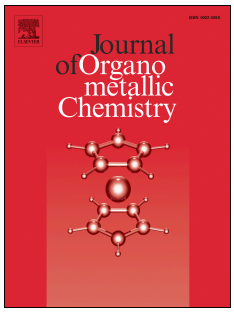

Efficient organic light-emitting diodes with low efficiency roll-off using iridium emitter with 2-(5-phenyl-1,3,4-oxadiazol-2-yl)phenol as ancillary ligand

Yi-Ming Jin , Cheng-Cheng Wang , Li-Sha Xue , Tian-Yi Li , Song Zhang , Xuan Liu , Xiao Liang , You-Xuan Zheng , Jing-Lin Zuo

PII: S0022-328X(14)00212-5

DOI: 10.1016/j.jorganchem.2014.04.030

Reference: JOM 18565

To appear in: *Journal of Organometallic Chemistry*

Received Date: 26 February 2014

Revised Date: 28 April 2014

Accepted Date: 28 April 2014

Please cite this article as: Y.-M. Jin, C.-C. Wang, L.-S. Xue, T.-Y. Li, S. Zhang, X. Liu, X. Liang, Y.-X. Zheng, J.-L. Zuo, Efficient organic light-emitting diodes with low efficiency roll-off using iridium emitter with 2-(5-phenyl-1,3,4-oxadiazol-2-yl)phenol as ancillary ligand, *Journal of Organometallic Chemistry* (2014), doi: 10.1016/j.jorganchem.2014.04.030.

Graphical abstract (synopsis)

Three new heteroleptic iridium(III) complexes with 1,3,4-oxadiazol containing ancillary ligands were synthesized and the OLEDs using one emitter showed superior performances with a peak current efficiency (η_c) of 61.49 cd A^{-1} and low efficiency roll-off.

Graphical Abstract (pictogram)

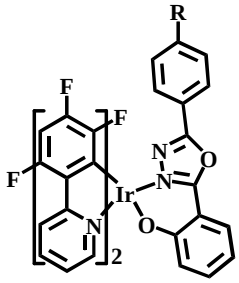

R = H: Ir($F_{3,4,6}$ppy)$_2$POP
R = F: Ir($F_{3,4,6}$ppy)$_2$FPOP
R = CF_3: Ir($F_{3,4,6}$ppy)$_2$$CF_3$POP

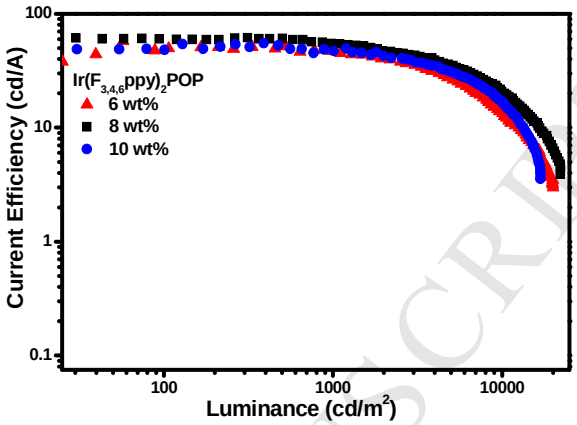

Efficient organic light-emitting diodes with low efficiency roll-off using iridium emitter with 2-(5-phenyl-1,3,4-oxadiazol-2-yl)phenol as ancillary ligand

Yi-Ming Jin, Cheng-Cheng Wang, Li-Sha Xue, Tian-Yi Li, Song Zhang, Xuan Liu, Xiao Liang, You-Xuan Zheng,* Jing-Lin Zuo

State Key Laboratory of Coordination Chemistry, Nanjing National Laboratory of Microstructures, Center for Molecular Organic Chemistry, School of Chemistry and Chemical Engineering, Nanjing University, Nanjing 210093, P. R. China, e-mail: yxzheng@nju.edu.cn

Yi-Ming Jin and Cheng-Cheng Wang are co-first author

Abstract

Using 2,4,5-trifluorophenylpyridine as a monoanionic cyclometalated ligand, 2-(5-phenyl-1,3,4-oxadiazol-2-yl)phenol, 2-(5-(4-fluorophenyl)-1,3,4-oxadiazol-2-yl)phenol and 2-(5-(4-trifluoro-methylphenyl)-1,3,4-oxadiazol-2-yl)phenol as ancillary ligands, three new heteroleptic iridium(III) complexes (**Ir($F_{3,4,6}$ppy)$_2$POP**, **Ir($F_{3,4,6}$ppy)$_2$FPOP** and **Ir($F_{3,4,6}$ppy)$_2$$CF_3$POP**) were developed. All complexes are green phosphors (λ_{max} = 503 - 521 nm) with photoluminescence quantum efficiency yields of 12 - 18% in CH_2Cl_2 solutions at room temperature, respectively. The organic light emitting diodes (OLEDs) with the structure of ITO / TAPC (1,1-bis(4-(di-*p*-tolylamino)phenyl)cyclohexane, 60 nm) / **Ir($F_{3,4,6}$ppy)$_2$POP** (6, 8, 10 wt%) : SimCP2 (bis(3,5-di(9*H*-carbazol-9-yl)phenyl)diphenylsilane, 30 nm) / TPBi (1,3,5-tri(1-phenyl-1*H*-benzo[d]imidazol-2-yl)phenyl, 90 nm) / LiF (1 nm) / Al (100 nm) showed good performances. Particularly, the device with 8 wt% doped concentration exhibited superior performances with a peak current efficiency (η_c) of 61.49 cd A^{-1} and a peak power efficiency (η_p) of 46.03 lm W^{-1}. Furthermore, the efficiency roll-off ratios from the peak current efficiency to that at the practical luminance of 100 cd m^{-2} and from 100 cd m^{-2} to the benchmark brightness of 1000 cd m^{-2} in this device are low, which are helpful to keep high efficiency at relatively high current density and high luminance.

Keywords: Iridium complex; 2,4,5-Trifluorophenylpyridine; 1,3,4-Oxadiazole; Organic light emitting diode; Efficiency

1. Introduction

Phosphorescent iridium complexes play an important part in efficient organic light emitting diodes (OLEDs) due to the high quantum efficiency and short lifetime of triplet excited states [1-20]. The strong spin-orbit coupling (SOC) introduced by the central heavy atom can promote the triplet to singlet radiative transition, so that such complexes may exhibit unusually high phosphorescence quantum yields at room temperature. On the other hand, since the phosphorescence of iridium complexes primarily originates from the metal-to-ligand charge transfers (MLCT) and the ligand-centered (LC) transitions [21], the energy level of the excited state can be controlled by tuning the energy levels of the ligands through substituent effects, which leads to a wide flexible emission color range.

In this context, heteroleptic cyclometalated (C^N) iridium(III) complexes ($(C^N)_2Ir(LX)$, LX = ancillary ligand) are promising phosphorescent materials due to easy synthetic chemical accessibility compared with the corresponding homoleptic $Ir(C^N)_3$ complexes and good photophysical properties [22-24]. According to the density functional theory calculation, the highest occupied molecular orbital (HOMO) is basically centered on the Ir(III) metal while the lowest unoccupied molecular orbital (LUMO) is generally localized on the cyclometalated ligands. Although most ancillary ligands do not make contribution to the lowest excited state directly, they indeed alter the energy levels of the excited states by modifying the electron density at the metal center. Thus, the photophysical property and carrier mobility of iridium complexes can be tuned trough functional substitutes on both cyclometalated and ancillary ligands. Our group has reported high efficient phosphorescent OLEDs by introducing tetraphenylimidodiphosphinate (tpip) derivatives as ancillary ligands into Ir(III) complexes [25-29]. Tpip derivatives have stronger polar P=O bonds, which may improve the electron mobility of the Ir(III) complexes, broaden the electron-hole recombination zone, balance the distribution of holes / electrons and reduce leakage current, particularly for the high doping concentration, leading to the suppressed the triplet-triplet annihilation (TTA) and triplet-polaron annihilation (TPA) effects in the device [30-32]. Therefore, Ir(III) complexes attached ancillary ligands with good electron mobility are potential efficient emitters for OLEDs.

1,3,4-Oxadiazole derivatives are good candidates for electron injection and transport materials due to their high electron affinity, high photoluminescence quantum yield and good thermal/chemical stability. Yang and Ma et. al. [33,34], Tian et. al. [35], Bryce et. al. [36] and our group [37] have reported efficient iridium complexes and devices using 1,3,4-oxadiazole derivatives as cyclometalated ligands to increase the complexes' electron transporting ability and consequently facilitate charge trapping across the bulk for high performance OLEDs. However, few heteroleptic Ir(III) complexes using 1,3,4-oxadiazole derivatives as ancillary ligands have been reported [38,39]. In addition, fluorination can enhance the electron mobility and result in a better balance of charge injection and transfer, lower vibrational frequency of C-F bond can reduce the rate of radiationless deactivation. On this basis, as shown in Scheme 1, we synthesized three heteroleptic Ir(III) complexes using 2,4,5-trifluorophenylpyridine (**$F_{3,4,6}$ppy**) as the cyclometalated ligand and the 2-(5-phenyl-1,3,4-oxadiazol-2-yl)phenol and its fluoro/trifluoromethyl substituted derivatives, 2-(5-(4-fluorophenyl)-1,3,4-oxadiazol-2-yl)phenol and 2-(5-(4-trifluoromethyl-phenyl)-1,3,4-oxadiazol-2-yl)phenol, as the ancillary ligands. Here, we describe the results of our investigation on the synthesis, structural characterization and photoluminescence / electroluminescence properties of these Ir(III) complexes.

2. Experimental Section

2.1 Materials and measurements.

All reagents and chemicals were purchased from commercial sources and used without further purification. ^{1}H NMR spectra were measured on a Bruker AM 400 spectrometer or a Bruker AM 500 spectrometer. Mass spectrometry (MS) spectra were obtained with an electrospray ionization (ESI) mass spectrometer (LCQ Fleet, Thermo Fisher Scientific) or matrixassisted laser desorption ionization time-of-flight (MALDI-TOF) mass spectrometer (Bruker Daltonic Inc.). Absorption and photoluminescence spectra were measured on a UV-3100 spectrophotometer and a Hitachi F-4600 photoluminescence spectrophotometer, respectively. The decay lifetimes were measured with an Edinburgh FLS-920 spectrometer in degassed CH_2Cl_2 solution at room temperature. Cyclic voltammetry measurements were conducted on a MPI-A multifunctional electrochemical and chemiluminescent system (Xi'an Remex Analytical Instrument Ltd. Co., China) at a scan rate 0.1 V s^{-1}, with a polished Pt plate as the working electrode, platinum thread as the counter

electrode and Ag-$AgNO_3$ (0.1 M) in CH_3CN as the reference electrode, *tetra*-n-butylammonium perchlorate (0.1 M) as the supporting electrolyte, together with Fc^+/Fc as the internal standard.

The luminescence quantum efficiencies were calculated by comparison of the emission intensities (integrated areas) of a standard sample (*fac*-Ir(ppy)$_3$) and the iridium complexes according to the equation (1) [40].

$$\Phi_{unk} = \Phi_{std}(\frac{I_{unk}}{I_{std}})(\frac{A_{std}}{A_{unk}})(\frac{\eta_{unk}}{\eta_{std}})^2 \qquad (1)$$

where Φ_{unk} and Φ_{std} are the luminescence quantum yields of the iridium complexes and *fac*-Ir(ppy)$_3$ (0.4 [41]), respectively. The I_{unk} and I_{std} are the integrated emission intensities of the iridium complexes and *fac*-Ir(ppy)$_3$ solution, respectively. The A_{unk} and A_{std} are the absorbance values of the iridium complexes and *fac*-Ir(ppy)$_3$ solution at their excitation wavelengths, respectively. The η_{unk} and η_{std} terms represent the refractive indices of the corresponding solvents (pure solvents were assumed).

2.2 Crystallography.

The single crystal structures of complexes were carried out on a Bruker SMART CCD diffractometer using monochromated Mo Kα radiation (λ = 0.71073 Å) at room temperature. Cell parameters were retrieved using the SMART software and refined using the SAINT program [42] on all observed reflections. Data were collected using a narrow-frame method with a scan width of 0.30° in ω and an exposure time of 10 s/frame. The highly redundant data sets were reduced using the SAINT program and corrected for Lorentz and polarization effects. Absorption corrections were applied using the SADABS program [43] supplied by Bruker. The structures were solved by direct methods and refined by full-matrix least-squares on *F*2 using the SHELXS-97 program [44]. The positions of metal atoms and their first coordination spheres were located from direct-methods E-maps; other non-hydrogen atoms were found in alternating difference Fourier syntheses and least-squares refinement cycles and refined anisotropically during the final cycles. Hydrogen atoms were placed in calculated position and refined as riding atoms with a uniform value of Uiso.

2.3 OLEDs fabrication and measurement.

All OLEDs with the emission area of 0.1 cm^2 were fabricated on the pre-patterned ITO-coated glass substrate with a sheet resistance of 15 Ω sq^{-1}. The 60 nm hole-transporting material of TAPC (1,1-bis(4-(di-*p*-tolylamino)phenyl)cyclohexane) film was first deposited on the ITO glass substrate. The phosphor and SimCP2 (bis(3,5-di(9*H*-carbazol-9-yl)phenyl)diphenylsilane) host were co-evaporated to form 30 nm emitting layer from two separate sources. To optimize the best device performances, the different doped concentrations of the Ir(III) complex in the host (6, 8, 10 wt%) were applied. Successively, TPBi (1,3,5-tri(1-phenyl-1*H*-benzo[d]imidazol-2-yl)phenyl, 90 nm), LiF (1 nm), and Al (100 nm) were evaporated. The vacuum was less than 1×10^{-4} Pa during all materials deposition. The electroluminescence spectra were measured with a Hitachi F-4600 photoluminescence spectrophotometer. The EL characteristic curves were measured with a computer controlled Keithley 2400 source meter with a calibrated silicon diode in air without device encapsulation.

2.4 Syntheses.

The syntheses procedures of ligands were listed in Scheme 1. The cyclometallated ligand (**$F_{3,4,6}$ppy**), cyclometallated Ir(III) chloro-bridged dimer (**[($F_{3,4,6}$ppy)$_2$Ir(μ-Cl)]$_2$**) and ancillary ligand (**HPOP**) were synthesized according to our previous report [29,39]. All reactions were performed under nitrogen. Solvents were carefully dried and distilled from appropriate drying agents prior to use.

2.4.1 Synthesis of the ancillary ligands (HLX).

5-Fluoro-benzoyl chloride (1.58 g, 10 mmol) was added dropwise to a solution of 2-methoxybenzohydrazine (1.66 g, 10 mmol) and triethylamine (1.01 g, 10 mmol) in chloroform (20 mL) at room temperature. The mixture was stirred for 2 h and then filtered. The solid was washed with water and ethanol to give *N*-(4-fluorobenzoyl)-2-methoxybenzohydrazine (2.59 g, 90% yield). A mixture of *N*-(4-fluorobenzoyl)-2-methoxybenzo-hydrazine and $POCl_3$ (20 mL) in a 50 mL flask was refluxed under nitrogen for 5 h. The excessive $POCl_3$ was then distilled out, and the residue was poured into water. The crude solid product was purified by recrystallization from chloroform/hexane to give 2-(4-fluorophenyl)-5-(2-methoxyphenyl)-1,3,4-oxadiazole (2.30 g, 85% yield). Then, to a mixture of 2-(4-fluorophenyl)-5-(2-methoxyphenyl)-1,3,4-oxadiazole (2.30

g) in 50 mL CH_2Cl_2 at -78 °C was added BBr_3 (12.5 g, 50 mmol in 20 mL CH_2Cl_2) dropwise. The mixture was stirred for 24 h at -78 °C and the resulting solution was poured into water, extracted with CH_2Cl_2 (50 mL × 3 times) and then dried over anhydrous sodium sulfate. The solvent was removed under reduced pressure, and recrystallization of the residue from ethanol gave colorless crystal of 2-(5-(4-fluoro-phenyl)-1,3,4-oxadiazol-2-yl)phenol (**HFPOP)** with a 87% yield. ^{1}H NMR (500 MHz, DMSO-d_6) δ 8.10 (dd, *J* = 8.4, 5.5 Hz, 2H), 7.74 (d, *J* = 7.6 Hz, 1H), 7.49 – 7.39 (m, 2H), 7.25 (t, *J* = 7.5 Hz, 1H), 6.90 (d, *J* = 8.4 Hz, 1H), 6.63 (t, *J* = 7.3 Hz, 1H).

2-(5-(4-Trifluoromethyl-phenyl)-1,3,4-oxadiazol-2-yl)phenol **(HCF$_3$POP)** was synthesized with the same procedure with 92% yield. ^{1}H NMR (500 MHz, $CDCl_3$) δ 8.29 (d, *J* = 8.1 Hz, 2H), 8.06 (dd, *J* = 7.7, 1.6 Hz, 1H), 7.82 (d, *J* = 8.2 Hz, 2H), 7.57 (t, *J* = 10 Hz, 2H), 7.16 – 7.10 (m, 2H).

2.4.2 General syntheses of complexes.

A mixture of $IrCl_3 \cdot 3H_2O$ (1 mmol) and **F$_{3,4,6}$ppy** (2.5 mmol) in 2-ethoxyethanol and water (20 mL, 3 : 1, v/v) was refluxed for 24 h. After cooling, the yellow solid precipitate was filtered to give the crude cyclometalated Ir(III) chloro-bridged dimer (**[(F$_{3,4,6}$ppy)$_2$Ir(μ-Cl)]$_2$**). Then the slurry of crude chloro-bridged dimer (0.2 mmol) and ancillary potassium salt (KLX, 0.5 mmol) in 2-ethoxyethanol (20 mL) was refluxed for 24 h. After the mixture was cooled, the solvent was evaporated at low pressure. The crude product was washed by water, and the column chromatography using CH_2Cl_2 as the eluent gave Ir(III) complexes which were further purified again by sublimation in vacuum.

Ir(F$_{3,4,6}$ppy)$_2$POP (yield: 56%): M.p. > 310 °C. ^{1}H NMR (500 MHz, DMSO-d_6) δ 8.65 (d, 1H), 8.44 (d, 1H), 8.17 (dd, *J* = 21.3 Hz, 2H), 8.01 – 7.86 (m, 4H), 7.83 (d, *J* = 6.5 Hz, 1H), 7.59 (dd, *J* = 16.0, 7.2 Hz, 1H), 7.33 (t, *J* = 6.4 Hz, 2H), 7.21 (t, *J* = 7.0 Hz, 1H), 7.12 (t, *J* = 6.6 Hz, 1H), 7.09 – 6.99 (m, 2H), 6.63 (d, *J* = 8.1 Hz, 1H), 6.53 (t, *J* = 7.5 Hz, 2H). MS(MALDI-TOF), m/z: calcd for $C_{36}H_{19}F_6IrN_4O_2$, 845.77 [M]; found 844.82 [M-1].

Ir(F$_{3,4,6}$ppy)$_2$FPOP (yield: 45%): M.p. >310 °C. ^{1}H NMR (500 MHz, DMSO-d_6) δ 8.64 (d, *J* = 5.6 Hz, 1H), 8.44 (d, *J* = 5.6 Hz, 1H), 8.18 (dd, *J* = 20.5, 8.5 Hz, 2H), 8.01 – 7.86 (m, 4H), 7.83 (d, *J* = 6.9 Hz, 1H), 7.42 (t, *J* = 8.7 Hz, 2H), 7.33 (t, *J* = 6.4 Hz, 1H), 7.21 (t, *J* = 7.0 Hz, 1H), 7.12 (t, *J* = 6.6 Hz, 1H), 7.09 – 6.99 (m, 2H), 6.63 (d, *J* = 8.6 Hz, 1H), 6.53 (t, *J* = 7.5 Hz, 1H). MS(MALDI-TOF), m/z: calcd for $C_{36}H_{18}F_7IrN_4O_2$, 863.76 [M]; found 862.75 [M-1].

Ir($F_{3,4,6}$ppy)$_2$$CF_3$POP (yield: 30%): M.p.: 291 ^{o}C. ^{1}H NMR (500 MHz, DMSO-d_6) δ 8.64 (d, *J* = 5.6 Hz, 1H), 8.45 (d, *J* = 5.7 Hz, 1H), 8.18 (dd, *J* = 21.9, 8.4 Hz, 2H), 8.04 (d, *J* = 8.2 Hz, 2H), 7.93 (t, *J* = 8.9 Hz, 4H), 7.85 (d, *J* = 8.0 Hz, 1H), 7.33 (t, *J* = 6.5 Hz, 1H), 7.22 (t, *J* = 7.3 Hz, 1H), 7.12 (t, *J* = 6.6 Hz, 1H), 7.06 (td, *J* = 11.0, 6.0 Hz, 2H), 6.64 (d, *J* = 8.7 Hz, 1H), 6.54 (t, *J* = 7.4 Hz, 1H). MS(MALDI-TOF), m/z: calcd for $C_{37}H_{18}F_9IrN_4O_2$, 913.76 [M]; found 912.70[M-1].

3. Results and Discussion

3.1 Crystallography and thermal stability.

The single crystals suitable for X-ray diffraction study of two iridium phosphors, **Ir($F_{3,4,6}$ppy)$_2$POP** and **Ir($F_{3,4,6}$ppy)$_2$FPOP**, were obtained by controlled sublimation under high vacuum atmosphere. The ORTEP diagrams of these two complexes are depicted in Fig. 1. The corresponding crystallographic data were collected in Table 1 and the selected bond lengths and angles were listed in Table S1. The central iridium atom is chelated by two anionic C^N main ligands and one monoanionic bidentate N^O ancillary ligand. The coordination sphere presents a distorted octahedral geometry, with the *cis*-C,C and *trans*-N,N in chelating disposition. Concerning the designed ancillary ligands with three rings, the phenol ring and the oxadiazole ring chelate with the iridium center via the O atom and a N atom, respectively, forming a relatively rigid hexatomic coordination ring. The left free phenyl and 4-fluorophenyl ring present a rather obvious dihedral angel towards the other two rings, in order to minimizing the steric effect. The Ir-C and Ir-N bonds between iridium center and C^N main ligands are about 2.0 Å and the Ir-O1 bonds (2.1 Å) are the longest among all the coordination bonds.

The melting points of **Ir($F_{3,4,6}$ppy)$_2$POP**, **Ir($F_{3,4,6}$ppy)$_2$FPOP** and **Ir($F_{3,4,6}$ppy)$_2$$CF_3$POP** are 322, 326 and 291 ^{o}C, respectively. And they are thermally stable up to 406, 408 and 393 ^{o}C (5 wt% loss, Fig. 2), respectively, indicating that the compounds are potential emitting materials used for fabricating efficient and stable OLEDs with long lifetime.

3.2 Photophysical and electrochemical property.

The UV-vis absorption spectra of the **Ir($F_{3,4,6}$ppy)$_2$POP**, **Ir($F_{3,4,6}$ppy)$_2$FPOP** and **Ir($F_{3,4,6}$ppy)$_2$$CF_3$POP** complexes in degassed CH_2Cl_2 at 5×10^{-5} mol.L^{-1} are shown in Fig. 3(a), and the electronic absorption data are listed in Table 2. The complexes showed almost the similar

absorption spectra in the range of 230-450 nm. The intense bands at high energy (250-350 nm) are assign to spin-allowed ligand-centered ^{1}LC (π-π*) transitions of **$F_{3,4,6}$ppy** and 1,3,4-oxadiazole derivative ligands. The absorption bands observed at lower energies extending into the spectral region (350-450 nm) can be assigned to spin-allowed (π-π*) ligands along with contribution from metal-to ligand charge transfer MLCT transition. These MLCT bands are attributed to an effective mixing of charge-transfer transitions with higher lying spin-allowed transition on the ligands through strong spin-orbit coupling of iridium atom [45].

Photoluminescence measurements were conducted in deaerated CH_2Cl_2 solutions at room temperature (Fig. 3(b), Table 2). The complexes **Ir($F_{3,4,6}$ppy)$_2$POP**, **Ir($F_{3,4,6}$ppy)$_2$FPOP** and **Ir($F_{3,4,6}$ppy)$_2$$CF_3$POP** emit intense green phosphorescence with peaks maxima at 504, 503 and 521 nm, respectively, which are belong to the mixed MLCT and CT transitions. The major emission peaks of **Ir($F_{3,4,6}$ppy)$_2$POP** and **Ir($F_{3,4,6}$ppy)$_2$FPOP** are similar, indicating that the introducing of F atom in the ancillary ligand doesn't affect the excited state of the complex greatly. However, when the CF_3 moiety was introduced to the ancillary ligand, the maximum peak of **Ir($F_{3,4,6}$ppy)$_2$$CF_3$POP** red-shifts about 20 nm, suggesting the strong electron withdrawing unit CF_3 in the ancillary ligand has effect on the charge transfer process. Moreover, the quantum yields of the three complexes **Ir($F_{3,4,6}$ppy)$_2$POP**, **Ir($F_{3,4,6}$ppy)$_2$FPOP** and **Ir($F_{3,4,6}$ppy)$_2$$CF_3$POP** in solution are 18%, 12% and 13%, respectively. In addition, the lifetimes of complexes **Ir($F_{3,4,6}$ppy)$_2$POP**, **Ir($F_{3,4,6}$ppy)$_2$FPOP** and **Ir($F_{3,4,6}$ppy)$_2$$CF_3$POP** are in the range of microseconds of 1.83, 2.14 and 1.91 μs in CH_2Cl_2 solution (Table 2, Fig. S1), which are indicative of the phosphorescent origin for the excited states in each case.

The redox properties and HOMO/LUMO energy levels of the dopants are relative to the charge transport ability and the OLED structure. To calculate the HOMO/LUMO energy levels of the present heteroleptic iridium complexes, the electrochemical behaviours of them in degassed CH_2Cl_2 solution were investigated by using cyclic voltammetry (Fig. 4). The HOMO levels were calculated from the oxidation potentials and the LUMO levels were obtained from the HOMO data and band gap got from UV-vis spectra. The cyclic voltammograms of the complexes **Ir($F_{3,4,6}$ppy)$_2$POP**, **Ir($F_{3,4,6}$ppy)$_2$FPOP** and **Ir($F_{3,4,6}$ppy)$_2$$CF_3$POP** in the positive range show strong oxidation peaks, while the reduction peaks are not obvious, demonstrating that the redox process of the complexes is not reversible completely, which is also observed in related Ir(III)

complexes containing oxadiazole units [33-39]. From the Fig. 4 and Table 2 it is observed that the differences of the oxidation peaks and HOMO/LUMO values of the three complexes are neglectable suggesting that the introduction of the F/CF_3 units has little effects on the the HOMO/LUMO levels.

3.3 OLEDs characterization

Because HOMO/LUMO levels of the three complexes are similar and the complex **Ir($F_{3,4,6}$ppy)$_2$POP** shows the highest PL efficiency, the OLEDs using **Ir($F_{3,4,6}$ppy)$_2$POP** as the emitter were fabricated with the structure of ITO / TAPC (60 nm) / **Ir($F_{3,4,6}$ppy)$_2$POP** (6, 8, 10 wt%) : SimCP2 (30 nm) / TPBi (90 nm) / LiF (1 nm) / Al (100 nm) named G1 – G3, respectively. TAPC and SimCP2 were employed as the hole-transporting layer and bipolar host material, respectively. TPBi was used as an electron-transporting and hole-blocking layer. The energy diagrams of the devices and the molecular structures of the materials used are shown in Fig. 5. Obviously, the HOMO/LUMO levels of **Ir($F_{3,4,6}$ppy)$_2$POP** are all within that of host material SimCP2. So, a good carrier trapping is expected in these devices, which is the dominated EL mechanism. Furthermore, holes and electrons will be well confined within the doped light-emitting layer.

The current efficiency (η_c) versus current density (J), power efficiency (η_p) versus J, J versus driving voltage (V), and η_c versus luminance (L) characteristics of devices are shown in Fig. 6. The key EL data are summarized in Table 3. All devices emit green light with the EL emission peaks at 504 nm for G1 – G3, closing to the PL spectrum of the **Ir($F_{3,4,6}$ppy)$_2$POP** complex in CH_2Cl_2 solution. The EL emission spectrum shapes are almost invariant of the current density and also do not show any concentration dependent, indicating that the EL emission of the device originates from the triplet excited states of the phosphor and the energy can be transferred from SimCP2 to the emitter [33].

The OLEDs using **Ir($F_{3,4,6}$ppy)$_2$POP** as the emitter exhibit encouraging EL performances, displaying low turn-on voltages of 3.4 - 3.5 V and high efficiency. The maximum $\eta_{c,max}$ and $\eta_{p,max}$ of G1 – G3 are in the range of 55.13 – 61.49 cd A^{-1} and 39.52 – 46.03 lm W^{-1}, respectively. According to the respective device, the $\eta_{c,max}$ and $\eta_{p,max}$ of 57.27 cd A^{-1} and 41.82 lm W^{-1} were obtained in G1 (6 wt%) at 4.3 V. The device G2 with 8 wt% dopant concentration showed the best

performances with a $\eta_{c,max}$ of 61.49 cd A^{-1} (4.9 V) and a $\eta_{p,max}$ of 46.03 lm W^{-1} (4.1 V). For the device G3, it showed the comparative values to that of G1 with a $\eta_{c,\,max}$ of 55.13 cd A^{-1} at 4.7 V and a $\eta_{p,\,max}$ of 39.52 lm W^{-1} at 3.9 V. The results suggested that for this device structure, the optimized doped concentration is 8 wt%.

Gratifyingly, from the Fig. 6 and Table 3 it is also can be observed that the efficiency roll-off in these devices is low, which is helpful to keep high efficiency at relatively high current density and high luminance. For device G1, the roll-off ratios of efficiency from the peak value (57.27 cd A^{-1}) to that at the practical brightness of 100 cd m^{-2} (49.59 cd A^{-1}) and from 100 cd m^{-2} to the benchmark brightness of 1000 cd m^{-2} (46.63 cd A^{-1}) are 13.4% and 6.0%, respectively. For device G2, efficiency roll-off ratios from the peak value (61.49 cd A^{-1}) to that at the brightness of 100 cd m^{-2} (59.81 cd A^{-1}) and from the brightness of 100 cd m^{-2} to 1000 cd m^{-2} (54.56 cd A^{-1}) are as low as 2.7% and 8.8%, respectively. For device G3, the efficiency roll-off ratios from the peak value (55.13 cd A^{-1}) to that at the brightness of 100 cd m^{-2} (51.21 cd A^{-1}) and from the brightness of 100 cd m^{-2} to 1000 cd m^{-2} (43.73 cd A^{-1}) are as low as 2.0% and 2.3%, respectively.

The good EL properties should be partly due to the application of 2-(5-phenyl-1,3,4-oxadiazol-2-yl)phenol as the ancillary ligand and 2,4,5-trifluorophenylpyridine as cyclometalated ligand. The dopant acts as the hole and electron traps to retard the motion of both types of carriers. The lower LUMO levels of the dopants are particularly important for the reason that the hole mobility of the TAPC is high than the electron mobility of the TPBi in OLEDs [46], the exciton accumulation is expected in hole blocking layer (TPBi) near the interface of emitting layer (**Ir($F_{3,4,6}$ppy)$_2$POP** : SimCP2) / TPBi) due to the high energy barrier between TPBi and SimCP2 [47]. The accumulation of exciton will cause the serious triplet-triplet annihilation (TTA), triplet-polaron annihilation (TPA) of the iridium complexes, and high efficiency roll-off consequently. In our case, the 1,3,4-oxadiazole units, as part of the ligand framework, will benefit the electron transport properties. The good electron mobility of the phosphorescent emitter would facilitate the injection and transport of electrons, which broaden the recombination zone, balance the distribution of holes and electrons, and reduce leakage current, particularly for the high doping concentration, leading to the suppressed the TTA, TPA effects [48,49], improved recombination probability and high device efficiency, low efficiency roll-off.

4. Conclusion

In conclusion, three new heteroleptic iridium(III) complexes using 2,4,5-trifluorophenylpyridine as a monoanionic cyclometalated ligand, 2-(5-phenyl-1,3,4-oxadiazol-2-yl)phenol, 2-(5-(4-fluorophenyl)-1,3,4-oxadiazol-2-yl)phenol and 2-(5-(4-trifluoromethylphenyl)-1,3,4-oxadiazol-2-yl)phenol as ancillary ligands were synthesized. Efficient EL devices ITO / TAPC (60 nm) / **Ir($F_{3,4,6}$ppy)$_2$POP** (6, 8, 10 wt%) : SimCP2 (30 nm) / TPBi (90 nm) / LiF (1 nm) / Al (100 nm) were fabricated. A $\eta_{p,max}$ of 46.03 lm W^{-1} and a $\eta_{c,\,max}$ of 61.49 cd A^{-1} are achieved at 8 wt% dopant concentration. Furthermore, the efficiency roll-off ratios from the peak values to that at the practical luminance are low, which is helpful to keep high efficiency at relatively high current density and high luminance. The study demonstrates that the iridium complexes with 1,3,4-oxadiazole containing ancillary ligand are potential emitters for efficient OLEDs.

Acknowledgments

This work was supported by the National Natural Science Foundation of China (Grant 21371093), the Major State Basic Research Development Program (2011CB808704, 2013CB922101) and the Natural Science Foundation of Jiangsu Province (BK20130054).

References

[1] S.L. Lin, L.H. Chan, R.H. Lee, M.Y. Yen, W.J. Kuo, C.T. Chen, R.J. Jeng, Adv. Mater. 20 (2008) 3947.

[2] G.J. Zhou, C.L. Ho, W.Y. Wong, Q. Wang, D.G. Ma, L.X. Wang, Z.Y. Lin, T.B. Marder, A. Beeby, Adv. Funct. Mater. 18 (2008) 499.

[3] Y. Liu, K. Ye, Y. Fan, W. Song, Y. Wang, Z. Hou, Chem. Commun. (2009) 3699.

[4] W.-Y. Wong, C.-L. Ho, J. Mater. Chem. 19 (2009) 4457.

[5] W.-Y. Wong, C.-L. Ho, Coord. Chem. Rev. 253 (2009) 1709.

[6] F.L. Xiao, Y. Liu, Z.Y. Hu, Q. Gan, L. Wang, Z.L. Wen, M.X. Zhu, W.G. Zhu, Synth. Met. 159 (2009) 1308.

[7] G.J. Zhou, W.-Y. Wong, S. Suo, J. Photochem. Photobio. C: Photochem. Rev. 11 (2010) 133.

[8] Z.Q. Chen, Z.Q. Bian, C.H. Huang, Adv. Mater. 22 (2010) 1534.

[9] Y.F. Wang, H. Tan, Y. Liu, C.X. Jiang, Z.Y. Hu, M.X. Zhu, L. Wang, W.G. Zhu, Y. Cao, Tetrahedron 66 (2010) 1483.

[10] G.J. Zhou, W.-Y. Wong, X.L. Yang, Chem. Asian J. 6 (2011) 1706.

[11] Q. Wang, Y.T. Tao, X.F. Qiao, J.S. Chen, D.G. Ma, C.L. Yang, J.G. Qin, Adv. Funct. Mater. 21 (2011) 1681.

[12] S.M. Chen, G.P. Tan, W.Y. Wong, H.S. Kwok, Adv. Funct. Mater. 21 (2011) 3785.

[13] J.M. Fernández-Hernández, C.H. Yang, J.I. Beltrán, V. Lemaur, F. Polo, R. Fröhlich, J. Cornil, L.D. Cola, J. Am. Chem. Soc. 133 (2011) 10543.

[14] T. Peng, Y. Yang, H. Bi, Y. Liu, D.G. Ma, Z. Hou, Y. Wang, J. Mater. Chem. 21 (2011) 3551.

[15] H. Tan, J.T. Yu, K.X. Nie, J.H. Chen, X.P. Deng, Z.Y. Zhang, G.T. Lei, M.X. Zhu, Y. Liu, W.G. Zhu, Polymer 52 (2011) 4792.

[16] C.L. Ho, L.C. Chi, W.Y. Hung, W.J. Chen, Y.C. Lin, H. Wu, E. Mondal, G.J. Zhou, K.T. Wong, W.Y. Wong, J. Mater. Chem. 22 (2012) 215.

[17] R.D. Costa, E. Ortí, H.J. Bolink, F. Monti, G. Accorsi, N. Armaroli, Angew. Chem. Int. Ed. 51 (2012) 8178.

[18] F. Monti, F. Kessler, M. Delgado, J. Frey, F. Bazzanini, G Accorsi., N. Armaroli, H.J. Bolink, E. Ortí, R. Scopelliti, M.K. Nazeeruddin, E. Baranoff, Inorg. Chem. 52 (2013) 10292.

[19] X.L. Yang, G.J. Zhou, W.-Y. Wong, J. Mater. Chem. C 2 (2014) 1760.

[20] L. Ying, C.-L Ho, H. B. Wu, Y. Cao, W.-Y. Wong, Adv. Mater. 26 (2014) 2459.

[21] S. Lamansky, P. Djurovich, D. Murphy, F. Abdel-Razzaq, H.E. Lee, C. Adachi, P.E. Burrows, S.R. Forrest, M.E. Thompson, J. Am. Chem. Soc. 123 (2001) 4304.

[22] S. Lamansky, P. Djurovich, D. Murphy, F. Abdel-Razzaq, R. Kwong, I. Tsyba, M. Bortz, B. Mui, R. Bau, M.E. Thompson, Inorg. Chem. 40 (2001) 1704.

[23] Y. You, S.Y. Park, J. Am. Chem. Soc. 127 (2005) 12438.

[24] T.H. Kwon, H.S. Cho, M.K. Kim, J.W. Kim, J.J. Kim, K.H. Lee, S.J. Park, I.S. Shin, H. Kim, D.M. Shin, Y.K. Chung, J.I. Hong, Organometallics 24 (2005) 1578.

[25] Y.C. Zhu, L. Zhou, H.Y. Li, Q.L. Xu, M.Y. Teng, Y.X. Zheng, J.L. Zuo, H.J. Zhang, X.Z. You, Adv. Mater. 23 (2011) 4041.

[26] M.Y. Teng, S. Zhang, S.W. Jiang, X. Yang, C. Lin, Y.X. Zheng, L.Y. Wang, D. Wu, J.L. Zuo, X.Z. You, Appl. Phys. Lett. 100 (2012) 073303.

[27] H.Y. Li, L. Zhou, M.Y. Teng, Q.L. Xu, C. Lin, Y.X. Zheng, J.L. Zuo, H.J. Zhang, X.Z. You, J. Mater. Chem. C 1 (2013) 560.

[28] Q.L. Xu, C.C. Wang, T.Y. Li, M.Y. Teng, S. Zhang, Y.M. Jing, X. Yang, W.N. Li, C. Lin, Y.X. Zheng, J.L. Zuo, X.Z. You, Inorg. Chem. 52 (2013) 4916.

[29] C.C. Wang, Y.M. Jing, T.Y. Li, Q.L. Xu, S. Zhang, W.N. Li, Y.X. Zheng, J.L. Zuo, X.Z. You, X.Q. Wang, Eur. J. Inorg. Chem. (2013) 5683.

[30] J. Kalinowski, W. Stampor, J. Mezyk, M. Cocchi, D. Virgili, V. Fattori, P. Di Marco, Phys. Rev. B 66 (2002) 235321.

[31] W.S. Jeon, T.J. Park, S.Y. Kim, R. Pode, J. Jang, J.H. Kwon, Appl. Phys. Lett. 93 (2008) 063303.

[32] G.J. Zhou, W.-Y. Wong, B. Yao, Z.Y. Xie, L.X. Wang, J. Mater. Chem.18 (2008) 1799.

[33] L.Q. Chen, H. You, C.L. Yang, D.G. Ma, J.G. Qin, Chem. Commun. (2007) 1352.

[34 L.Q. Chen, C.L. Yang, M. Li, J.G. Qin, J. Gao, H. You, D.G. Ma, Cryst. Growth Des. 7 (2007) 39.

[35] Z. Xu, Y. Li, X. Ma, X. Gao, H. Tian, Tetrahedron 64 (2008) 1860.

[36] Y.H. Zheng, A.S. Batsanov, M.R. Bryce, Inorg. Chem. 50 (2011) 3354.

[37] Q.L. Xu, H.Y. Li, C.C. Wang, S. Zhang, T.Y. Li, Y.M. Jing, Y.X. Zheng, W. Huang, J.L. Zuo, X.Z. You, Inorg. Chim. Acta 391 (2012) 50.

[38] H.R. Park, B.Y. Kim, Y.K. Kim, Y. Ha, J. Nanosci. Nanotechnol. 12 (2012) 5613.

[39] H.Y. Li, T.Y. Li, M.Y. Teng, Q.L. Xu, S. Zhang, Y M. Jin, X. Liu, Y.X. Zheng, J.L. Zuo, J. Mater. Chem. C 2 (2014) 1116.

[40] D.P. Rillema, D.G. Taghdiri, D.S. Jones, C.D. Keller, L.A. Worl, T.J. Meyer, H. A. Levy, Inorg. Chem. 26 (1987) 578.

[41] K.A. King, P.J. Spellane, R.J. Watts, J. Am. Chem. Soc. 107 (1985) 1431.

[42] SAINT-Plus, version 6.02; Bruker Analytical X-ray System: Madison, WI (1999).

[43] G.M. Sheldrick, SADABS An empirical absorption correction program; Bruker Analytical X-ray Systems: Madison, WI (1996).

[44] G.M. Sheldrick, SHELXTL-97; Universität of Göttingen: Göttingen, Germany (1997).

[45] Y.T. Tao, C.L. Yang, J.G. Qin, Chem. Soc. Rev. 40 (2011) 2943.

[46] H.H. Fong, K.C. Lun, S.K. So, Chem. Phys. Lett. 353 (2002) 407.

[47] I.D. Parker, J. Appl. Phys. 75 (1994) 1656.

[48] J. Kalinowski, W. Stampor, J. Mezyk, M. Cocchi, D. Virgili, V. Fattori, P. Di Marco, Phys. Rev. B 66 (2002) 235321.

[49] W.S. Jeon, T.J. Park, S.Y. Kim, R. Pode, J. Jang, J.H. Kwon, Appl. Phys. Lett. 93 (2008) 063303.

Table captions

Table 1 Crystallographic data for **Ir($F_{3,4,6}$ppy)$_2$POP** and **Ir($F_{3,4,6}$ppy)$_2$FPOP**.

Table 2. The photophysical properties of complexes **Ir($F_{3,4,6}$ppy)$_2$POP**, **Ir($F_{3,4,6}$ppy)$_2$FPOP** and **Ir($F_{3,4,6}$ppy)$_2$CF_3POP**.

Table 3. EL performances of devices G1 - G3.

Table 1 Crystallographic data for **Ir($F_{3,4,6}$ppy)$_2$POP** and **Ir($F_{3,4,6}$ppy)$_2$FPOP**.

	Ir($F_{3,4,6}$ppy)$_2$POP	**Ir($F_{3,4,6}$ppy)$_2$FPOP**
Formula	$C_{36}H_{19}F_6IrN_4O_2$	$C_{36}H_{18}F_7IrN_4O_2$
FW	845.77	863.76
T (K)	296(2)	296(2)
Wavelength (Å)	0.71073	0.71073
Cryst syst	Monoclinic	Monoclinic
Space group	$P2_1/n$	$P2_1/c$
a (Å)	11.2437(5)	11.3459(4)
b (Å)	15.6194(7)	18.0095(7)
c (Å)	17.6047(8)	15.7264(6)
a (deg)	90.00	90.00
β (deg)	1100.1100(10)	107.3820(10)
γ (deg)	90.00	90.00
V (Å^3)	3043.7(2)	3066.7(2)
Z	4	4
ρ_{calcd} (g/cm^3)	1.846	1.871
μ (Mo Kα) (mm^{-1})	4.465	4.439
F (000)	1640	1672
Range of transm factors (deg)	1.76 -28.42	1.77 -28.32
Reflns collected	21911	21789
Unique	7629	7636
GOF on F^2	1.009	1.024
$R_1{}^a$,$wR_2{}^b$ (I>2s(I))	0.0238, 0.0546	0.0293, 0.0654
$R_1{}^a$,$wR_2{}^b$ (all data)	0.0317, 0.0578	0.0404, 0.0678
CCDC NO.	934801	934802

$R_1{}^a = \Sigma||F_o| - |F_c||/\Sigma F_o|$. $wR_2{}^b = [\Sigma w(F_o{}^2 - F_c{}^2)^2/\Sigma w(F_o{}^2)]^{1/2}$

Table 2. The photophysical properties of complexes **Ir($F_{3,4,6}$ppy)$_2$POP**, **Ir($F_{3,4,6}$ppy)$_2$FPOP** and **Ir($F_{3,4,6}$ppy)$_2$$CF_3$POP**.

Complex	T_m/T_d [a]	λ_{Abs} [b]	$\lambda_{em, RT}$ [b]	Φ [c]	τ [b]	HOMO/LUMO [d]
	[^{o}C]	[nm]	[nm]	[%]	[μs]	[eV]
Ir($F_{3,4,6}$ppy)$_2$POP	322/406	252/394	504/530	18	1.83	-5.59/-2.95
Ir($F_{3,4,6}$ppy)$_2$FPOP	326/408	253/393	503/530	12	2.14	-5.58/-2.92
Ir($F_{3,4,6}$ppy)$_2$$CF_3$POP	291/393	253/307	521	13	1.92	-5.58/-2.91

[a] T_m: melting point; T_d: decomposed temperature; [b] Measured in CH_2Cl_2 solution at room temperature; [c] Measured in degassed CH_2Cl_2 solution at room temperatureusing *fac*-Ir(ppy)$_3$ as the standard sample (Φ = 0.4); [d] HOMO/LUMO calculated based on the cyclovoltammety (CV) diagram using ferrocene as the internal standard and UV-vis spectra in dichloromethane. HOMO (eV) = -(E_{ox}-$E_{1/2,Fc}$)-4.8, LUMO (eV) = HOMO + $E_{bandgap}$.

Table 3. EL performances of devices G1 - G3.

Device	$V_{turn\text{-}on}$ [a]	$\eta_{p,\,max}$ [b] (lm W^{-1})	$\eta_{c,\,max}$ (cd A^{-1})			Current efficiency roll-off (%)	
	(V)	V	$\eta_{c,\,max}$ [c], V	100 [d]	1000 [e]	$\eta_{c,\,max}$ –100 cd/m^2 [f]	100–1000 cd/m^2 [g]
G1	3.5	41.82, 4.3	57.27, 4.3	49.59	46.63	13.4	6.0
G2	3.4	46.03, 4.1	61.49, 4.9	59.81	54.56	2.7	8.8
G3	3.4	39.52, 3.9	55.13, 4.7	51.21	43.73	2.0	2.3

[a] $V_{turn\text{-}on}$: turn-on voltage recorded at a brightness of 1 cd m^{-2}; [b] $\eta_{p,\,max}$: maximum power efficiency; [c] $\eta_{c,\,max}$: maximum current efficiency; [d] current efficiency at 100 cd m^{-2}; [h] current efficiency at 1000 cd m^{-2}; [f] Current efficiency roll-off (%) from peak value to 100 cd m^{-2}; [g] Current efficiency roll-off (%) from 100 cd m^{-2} to 1000 cd m^{-2}.

Scheme and figure captions

Scheme 1. The synthetic route of **Ir($F_{3,4,6}$ppy)$_2$POP**, **Ir($F_{3,4,6}$ppy)$_2$FPOP** and **Ir($F_{3,4,6}$ppy)$_2$$CF_3$POP**.

Fig. 1. ORTEP diagrams of **Ir($F_{3,4,6}$ppy)$_2$POP** (left) and **Ir($F_{3,4,6}$ppy)$_2$FPOP** (right) with thermal ellipsoids shown at 40% probability level. Labels are added on the atoms bonded to iridium center. Hydrogen atoms are omitted for clarity.

Fig. 2. The TG curves of **Ir($F_{3,4,6}$ppy)$_2$POP**, **Ir($F_{3,4,6}$ppy)$_2$FPOP** and **Ir($F_{3,4,6}$ppy)$_2$$CF_3$POP** complexes.

Fig. 3. UV-vis absorption (a) and emission (b) spectra of **Ir($F_{3,4,6}$ppy)$_2$POP**, **Ir($F_{3,4,6}$ppy)$_2$FPOP** and **Ir($F_{3,4,6}$ppy)$_2$$CF_3$POP** complexes in degassed dichloromethane (5×10^{-5} mol.L^{-1}) at room temperature.

Fig. 4. Cyclic voltammograms of complexes in the positive range.

Fig. 5. Energy level diagrams of HOMO and LUMO levels (relative to vacuum level) and molecular structures for materials investigated.

Fig. 6. Characteristics of devices with configuration ITO / TAPC (60 nm) / **Ir($F_{3,4,6}$ppy)$_2$POP** : SimCP2 (30 nm) / TPBi (90 nm) / LiF (1 nm) / Al (100 nm): (a) current efficiency (η_c) as a function of current density (J), (b) power efficiency (η_p) as a function of J, and (c) J versus driving voltage (V), (d) η_c versus luminance (L).

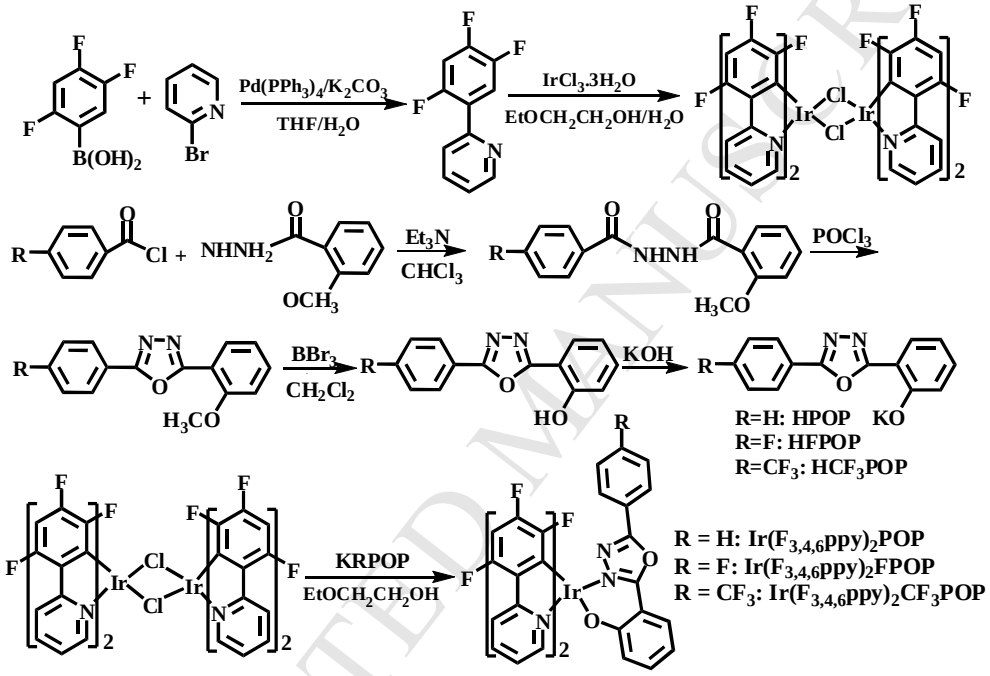

Scheme 1. The synthetic route of **Ir($F_{3,4,6}$ppy)$_2$POP**, **Ir($F_{3,4,6}$ppy)$_2$FPOP** and **Ir($F_{3,4,6}$ppy)$_2$CF$_3$POP**.

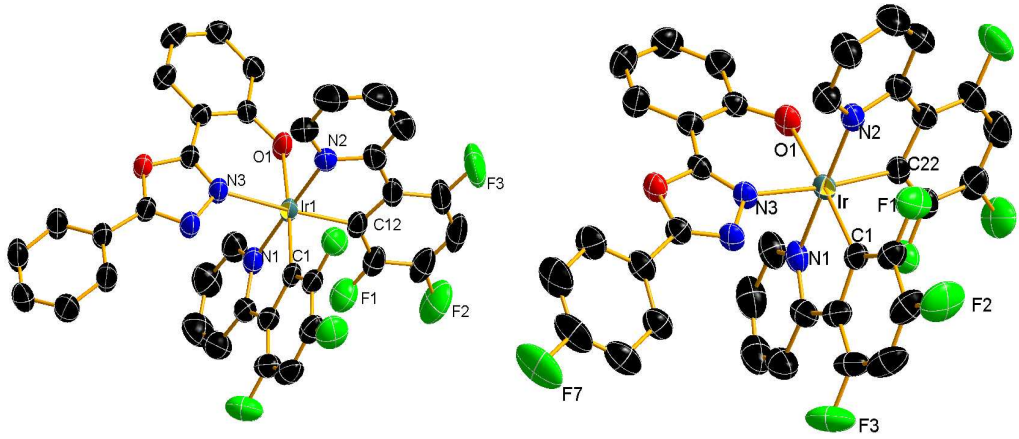

Fig. 1. ORTEP diagrams of **Ir($F_{3,4,6}$ppy)$_2$POP** (left) and **Ir($F_{3,4,6}$ppy)$_2$FPOP** (right) with thermal ellipsoids shown at 40% probability level. Labels are added on the atoms bonded to iridium center. Hydrogen atoms are omitted for clarity.

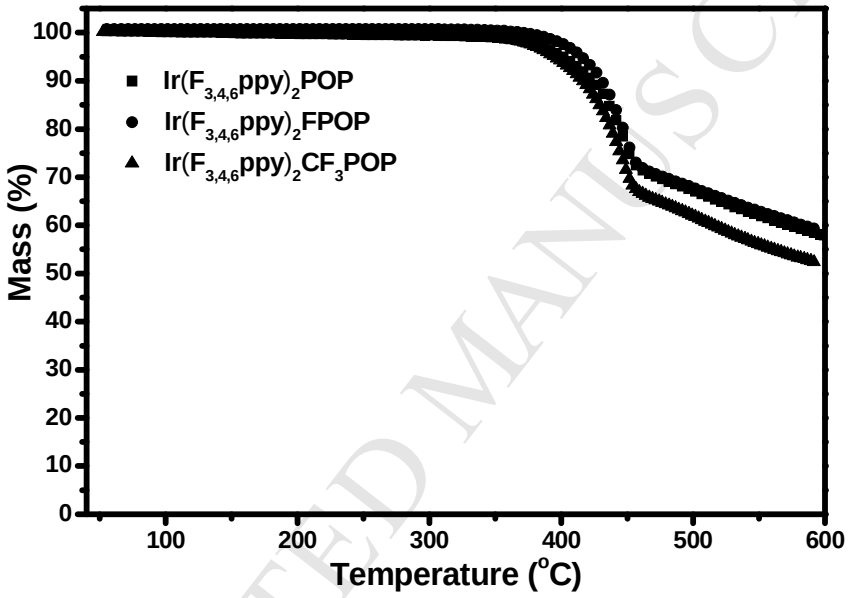

Fig. 2. The TG curves of **Ir($F_{3,4,6}$ppy)$_2$POP**, **Ir($F_{3,4,6}$ppy)$_2$FPOP** and **Ir($F_{3,4,6}$ppy)$_2$$CF_3$POP** complexes.

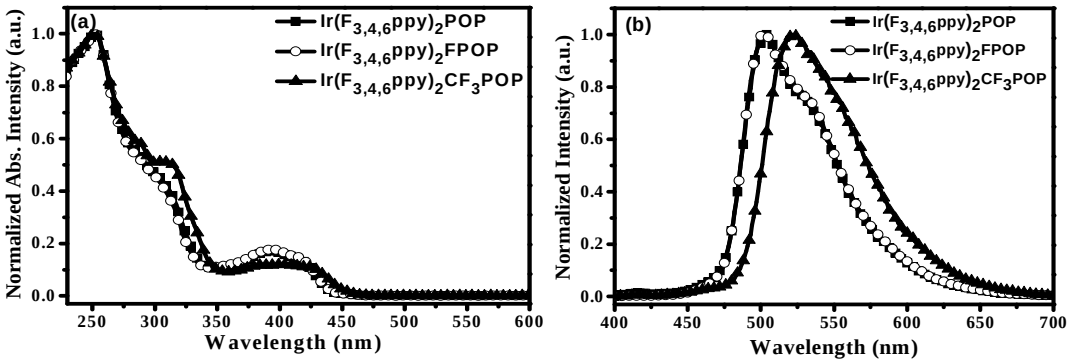

Fig. 3. UV-vis absorption (a) and emission (b) spectra of **Ir($F_{3,4,6}$ppy)$_2$POP**, **Ir($F_{3,4,6}$ppy)$_2$FPOP** and **Ir($F_{3,4,6}$ppy)$_2$$CF_3$POP** complexes in degassed dichloromethane (5×10^{-5} mol.L^{-1}) at room temperature.

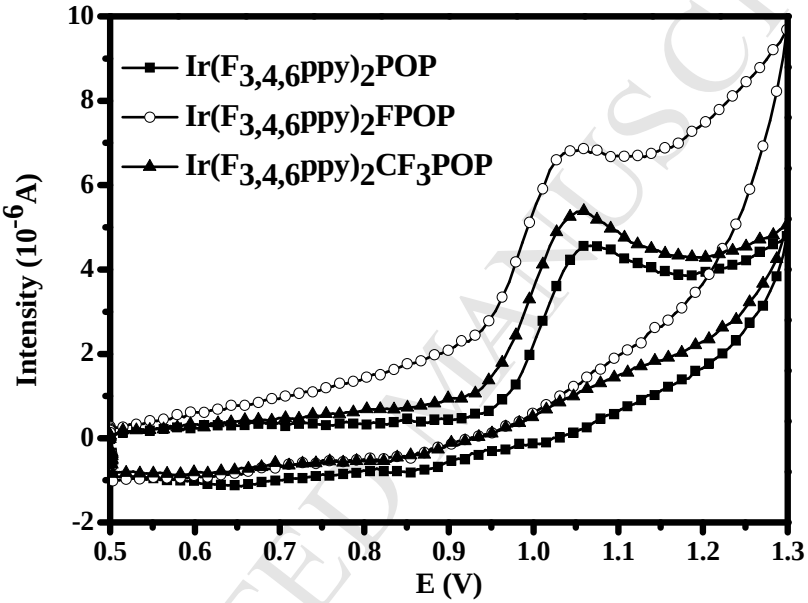

Fig. 4. Cyclic voltammograms of complexes in the positive range.

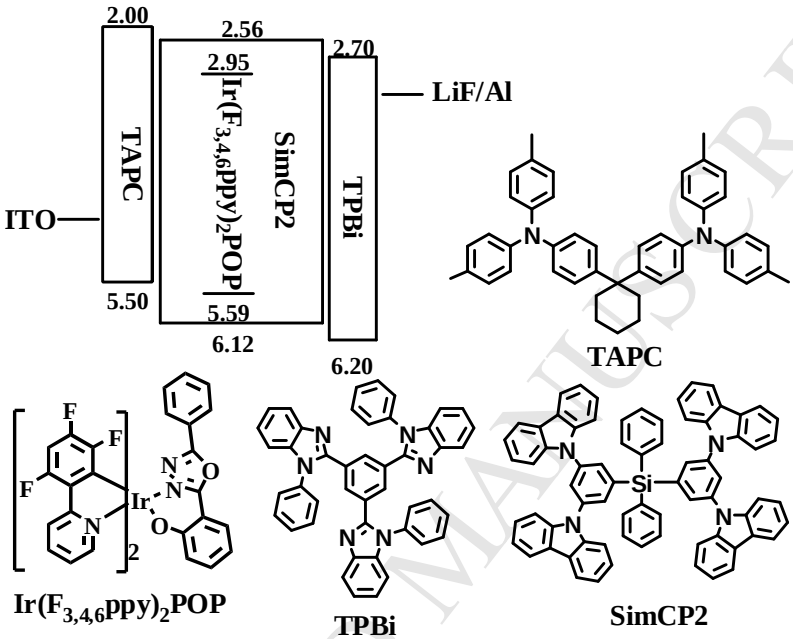

Fig. 5. Energy level diagrams of HOMO and LUMO levels (relative to vacuum level) and molecular structures for materials investigated.

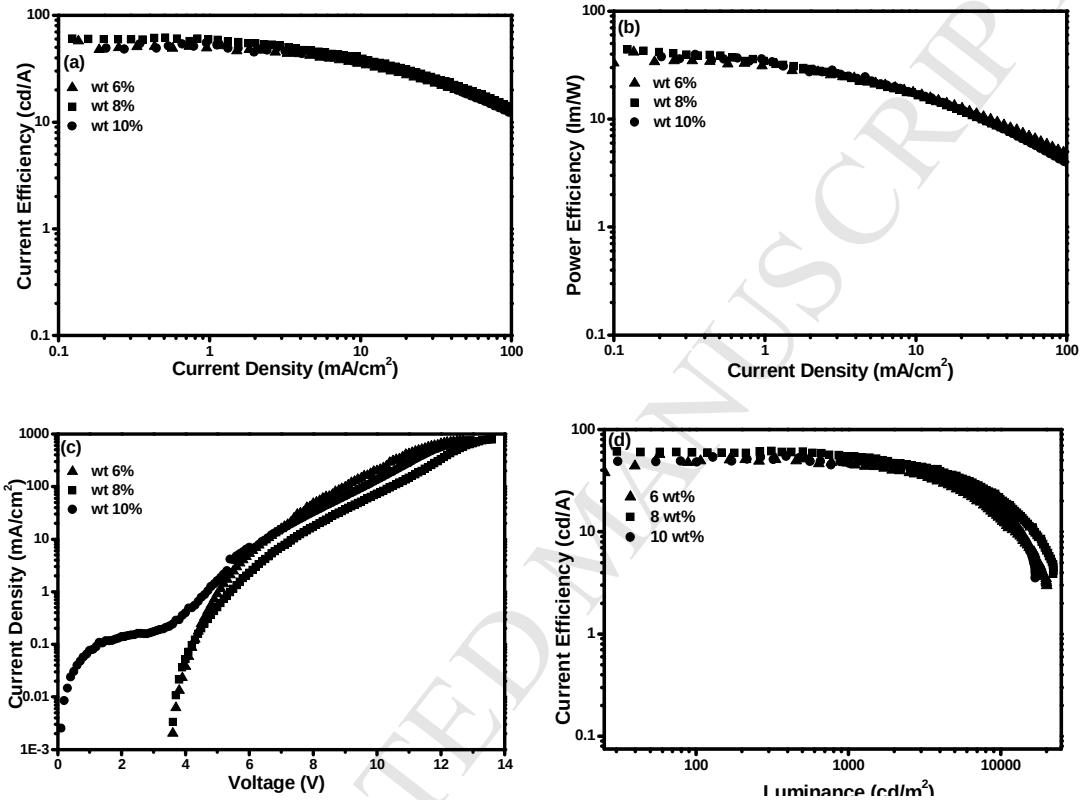

Fig. 6. Characteristics of devices with configuration ITO / TAPC (60 nm) / **Ir($F_{3,4,6}$ppy)$_2$POP** : SimCP2 (30 nm) / TPBi (90 nm) / LiF (1 nm) / Al (100 nm): (a) current efficiency (η_c) as a function of current density (J), (b) power efficiency (η_p) as a function of J, and (c) J versus driving voltage (V), (d) η_c versus luminance (L).

Research highlights

- We synthesize Ir(III) complexes with 1,3,4- oxadiazol derivatives.
- The complexes own green emission peaks with various intensities.
- One OLED shows a peak current efficiency of 61.49 cd A^{-1}.

Supporting Information

Efficient organic light-emitting diodes with low efficiency roll-off using iridium emitter with 2-(5-phenyl-1,3,4-oxadiazol-2-yl)phenol as ancillary ligand

Yi-Ming Jin, Cheng-Cheng Wang, Li-Sha Xue, Tian-Yi Li, Song Zhang, Xuan Liu, Xiao Liang, You-Xuan Zheng,* Jing-Lin Zuo

State Key Laboratory of Coordination Chemistry, Nanjing National Laboratory of Microstructures, Center for Molecular Organic Chemistry, School of Chemistry and Chemical Engineering, Nanjing University, Nanjing 210093, P. R. China, e-mail: yxzheng@nju.edu.cn

Yi-Ming Jin and Cheng-Cheng Wang are co-first author

Table S1. The selected bond lengths (Å) and angles (°) of **Ir($F_{3,4,6}$ppy)$_2$POP** and **Ir($F_{3,4,6}$ppy)$_2$FPOP** complexes.

Fig. S1. The lifetime decay curves of Ir($F_{3,4,6}$ppy)$_2$POP, Ir($F_{3,4,6}$ppy)$_2$FPOP and Ir($F_{3,4,6}$ppy)$_2$$CF_3$POP in CH_2Cl_2 solution.

Table S1. The selected bond lengths (Å) and angles (°) of **Ir($F_{3,4,6}$ppy)$_2$POP** and **Ir($F_{3,4,6}$ppy)$_2$FPOP** complexes.

Complex	Bond length (Å)		
Ir($F_{3,4,6}$ppy)$_2$POP	Ir(1)-C(1) 2.003(3)	Ir(1)-C(12) 2.019(3)	Ir(1)-N(1)2.034(2)
	Ir(1)-N(2) 2.038(3)	Ir(1)-N(3) 2.111(2)	Ir(1)-O(1) 2.1215(18)
	Angles (°)		
	C(1)-Ir(1)-C(12)89.04(10)	C(1)-Ir(1)-N(1) 80.22(11)	C(12)-Ir(1)-N(1) 98.76(11)
	C(1)-Ir(1)-N(2) 99.48(11)	C(12)-Ir(1)-N(2) 80.33(12)	N(1)-Ir(1)-N(2) 179.05(9)
	C(1)-Ir(1)-N(3) 93.29(9)	C(12)-Ir(1)-N(3) 177.21(10)	N(1)-Ir(1)-N(3) 83.16(9)
	N(2)-Ir(1)-N(3) 97.76(10)	C(1)-Ir(1)-O(1) 174.21(10)	C(12)-Ir(1)-O(1) 91.73(9)
	N(1)-Ir(1)-O(1) 93.99(9)	N(2)-Ir(1)-O(1) 86.31(9)	N(3)-Ir(1)-O(1) 86.11(8)
	Bond length (Å)		
Ir($F_{3,4,6}$ppy)$_2$FPOP	Ir(1)-C(1) 1.995(3)	Ir(1)-C(22) 2.011(3)	Ir(1) -N(1) 2.031(3)
	Ir(1)-N(2) 2.039(3)	Ir(1)-N(3) 2.105(3)	Ir(1)-O(1) 2.116(2)
	Angles (°)		
	C(1)-Ir(1)-C(22) 92.49(13)	C(1)-Ir(1)-N(1) 80.27(14)	C(22)-Ir(1)-N(1) 99.66(13)
	C(1)-Ir(1)-N(2) 99.64(13)	C(22)-Ir(1)-N(2) 79.73(13)	N(1)-Ir(1)-N(2) 179.38(11)
	C(1)-Ir(1)-N(3) 92.64(12)	C(22)-Ir(1)-N(3) 174.10(12)	N(1)-Ir(1)-N(3) 84.07(11)
	N(2)-Ir(1)-N(3) 96.54(11)	C(1)-Ir(1)-O(1) 173.97(12)	C(22)-Ir(1)-O(1) 88.02(12)
	N(1)-Ir(1)-O(1) 93.72(11)	N(2)-Ir(1)-O(1) 86.36(11)	N(3)-Ir(1)-O(1) 87.18(10)

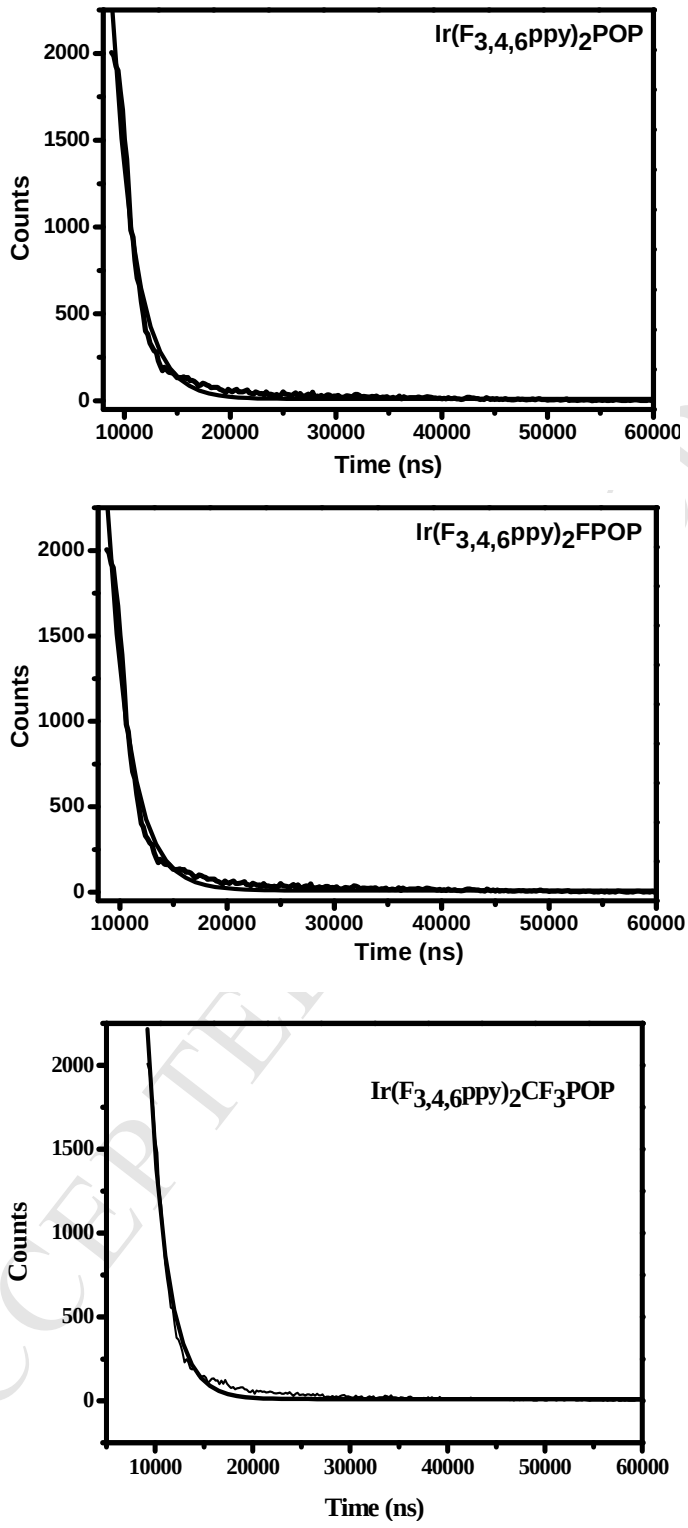

Fig. S1. The lifetime decay curves of **Ir($F_{3,4,6}$ppy)$_2$POP**, **Ir($F_{3,4,6}$ppy)$_2$FPOP** and **Ir($F_{3,4,6}$ppy)$_2$$CF_3$POP** in CH_2Cl_2 solution.